Acta Crystallographica Section A
Foundations of Crystallography
ISSN 0108-7673

Received 12 May 2000
Accepted 26 September 2000

Wavefunctions derived from experiment. II. A wavefunction for oxalic acid dihydrate

Daniel J. Grimwood* and Dylan Jayatilaka

Department of Chemistry, The University of Western Australia, Nedlands 6907, Australia. Correspondence e-mail: reaper@crystal.uwa.edu.au

A wavefunction has been derived for the oxalic acid dihydrate molecule using accurate low-temperature X-ray electron-density structure-factor data. The electron density from this constrained theoretical wavefunction is compared to those of unconstrained theoretical wavefunctions. Fitted electron densities around hydrogen atoms show significant deviation compared to Hartree–Fock calculations. In particular, hydrogen bonding appears enhanced in the crystal over theoretical predictions, while the density usually attributed to lone-pair electrons of the oxalic acid oxygen atoms is decreased. The constrained fitting procedure improves the overall agreement of the calculated structure factors even for structure factors that were not used as input to the fitting procedure. The pictures obtained from the constrained fitting procedure are insensitive to random errors introduced into the data. Similarly, the fitting procedure is able to reproduce features that arise from more accurate theoretical calculations. However, we are unable to fit our wavefunction to within the experimentally quoted error bounds without allowing an unreasonably large change in the energy of the constrained wavefunction. Large Hartree–Fock and density functional theory (DFT) cluster calculations involving up to 86 atoms in size also do not show significantly improved agreement with the experimentally observed structure factors. Derived properties from the constrained wavefunction fragments, such as the kinetic energy, electrostatic potential and the electron localization function, are also presented. In general, there are no difficulties in extracting experimental wavefunctions and the associated derived properties from elastic X-ray scattering data for crystal fragments of the order of 20 atoms.

1. Introduction

All physical measurements are related to integrals of certain operators over the square of an entity called the wavefunction. Normally, of course, the wavefunction is calculated by solving the Schrödinger equation. The Schrödinger equation is linked to the experimentally observed world through certain fundamental constants that appear in it.

In a previous article (Jayatilaka & Grimwood, 2001), hereafter called paper I, we have described in detail the possibility, philosophy and process of extracting a 'wavefunction' directly from experimental data – especially charge-density data obtained from elastic X-ray scattering experiments. Essentially, one starts from the point of view that a solution of the Schrödinger equation to an acceptable accuracy is too demanding to be practical. The direct incorporation of experimental data into the Schrödinger equation (or some well defined approximation to it) then becomes desirable for pragmatic considerations. The solution to such a modified Schrödinger equation is called an *experimental model wavefunction*.

The parameters in this experimental wavefunction are to be chosen according to a procedure that results in broad agreement with the experiment (according to some specified criteria) *and* to be reasonable according to some well defined approximation to the Schrödinger equation. In this way, one might be confident that properties calculated from such a wavefunction – particularly those properties not used in the constraint procedure – are closer to the actual properties of the system.

Scattering experiments are particularly well suited for an experimental wavefunction analysis, because they provide data concerning property densities associated with one particular state, and this information could be usefully incorporated into the Schrödinger equation for that state. This is quite different from the information obtained from spectroscopic experiments; the energy differences from the spectroscopic experiments may be built into the spectrum of a model or effective Hamiltonian but the eigenstates associated with this model Hamiltonian need have no direct connection with the 'real' eigenstates of the Schrödinger equation.

In paper I, a detailed and systematically improvable procedure for extracting wavefunctions from experimental X-ray data was proposed, suitable for the analysis of charge densities in molecular crystals. The non-interacting Hartree–Fock fragment wavefunction was proposed as a specific example of this procedure. The method has been successfully applied already to the charge density in the beryllium crystal (Jayatilaka, 1998), which has only one atom in the unit cell.

The purpose of this paper is to demonstrate that experimental wavefunctions can be straightforwardly extracted for molecular crystals with the order of 20 atoms in the unit cell. Here, we consider the oxalic acid dihydrate system, mainly because there is already extensive experimental X-ray information. The primary interest is in the effects of the constraint procedure in reconstructing the electron density from the X-ray information. Oxalic acid dihydrate is known to have strong hydrogen bonding and we will test whether or not these subtle effects can be extracted and, if present, whether these effects are reasonable. It is also of interest to see how these effects might compare to other models for analyzing the charge density. In addition, we will examine other related properties, such as the kinetic energy and the electron localization function, which cannot normally be extracted from standard charge-density analyses.

2. Theory and calculation details

2.1. Variational wavefunction fitting procedure

The theory for constraining a theoretical wavefunction from X-ray data has been discussed in detail in paper I. Briefly, the method for extracting wavefunctions from a given set of observed properties involves the following simple three-step procedure (Jayatilaka, 1998):

(I) Choose an appropriate variational *Ansatz* for the wavefunction (for example, one might choose the Hartree–Fock wavefunction).

(II) Calculate the desired experimental properties from this wavefunction and evaluate the agreement between the calculated and observed properties using a desired agreement statistic (for example, one might use the χ^2 statistic).

(III) If the agreement is not acceptable, use Lagrange's method to minimize the variational energy of the chosen wavefunction subject to an imposed *additional* constraint that the agreement statistic must have the desired (acceptable) value.

The method introduces a single additional Lagrange multiplier (usually written λ) whose value can be adjusted to constrain a given agreement statistic to have a desired (acceptable) value.

2.2. Data for the oxalic acid dihydrate crystal

Oxalic acid dihydrate crystallizes in the $P2_1/n$ space group with $Z = 2$. The atomic positions and thermal parameters used in our calculations are the high-angle set refined by Zobel and co-workers at 15 K (Zobel *et al.*, 1992), using the atomic form-factor method. The set of unique experimental structure factors was supplied by Zobel but are different to those deposited with the IUCr with their paper (Zobel *et al.*, 1992; Zobel, 1996). Following their method, structure factors F with $F < 2\sigma$, where σ is the estimated experimental error, were rejected from the data set. The structure factors supplied included secondary-extinction corrections.

As we are interested in electron density in regions not near the atomic positions (the so-called 'valence-electron' density), we consider only those measurements corresponding to low Fourier components, with $\sin\theta/\lambda < 0.71$ Å^{-1}, where θ is the X-ray scattering angle and λ is the X-ray wavelength. The cut-off 0.71 Å^{-1} is again used for consistency.

2.3. Details of wavefunction calculations

Most calculations were performed using the Hartree–Fock method on a fragment comprised of a central oxalic acid molecule surrounded by the four nearest water molecules. The orbitals for this fragment were expanded as a linear combination of Gaussian basis functions, using the double zeta plus polarization 'DZP' basis functions from the work of Dunning (1970). To see the importance of the size of the basis set, this was compared to the Dunning cc-pVTZ basis set (Dunning, 1989).

Hartree–Fock wavefunctions were constrained to the experimental data as described in paper I, using software written by us. The method of Tanaka (1988) was used to correct for the effect of thermal vibrational smearing of the electron density. Since the molecular fragment considered in this work is not equivalent to the symmetry-unique portion of the crystal (the asymmetric unit), the Gaussian exponent density partitioning method described in paper I was used to calculate the structure factors from the symmetry-redundant portions of the wavefunction.

Density-functional calculations were performed using the *Gaussian98* program (Frisch *et al.*, 1998), using the 'BLYP' method, comprised of Becke's exchange functional (Becke, 1988) with the correlation functional of Lee *et al.* (1988).

2.4. The promolecule model and density plots

The promolecule model is one where the density is assumed to be a sum of spherically averaged electron distributions for isolated atoms. The promolecule model is often used as a reference state; deviations from this model help to identify changes in the electron density due to chemical bonding. When calculating the 'deformation density', which is the difference between the calculated electron density and the promolecule model, only basis functions centered on the particular atom are used to calculate the atomic densities. In this work, the difference compared to using the full set of basis functions for the molecular fragment for each atom calculation (the so-called basis-set superposition error) was less than 1% for all points in the plots and deemed too small to distinguish. The spherically averaged electron densities for each atom were also calculated using the (unrestricted) Hartree–Fock method. Spherical symmetry was imposed on the Hartree–Fock calculation *post facto*, rather than being incorporated into the self-consistent field calculation (see, for

Table 1
χ^2 and R_w agreement statistics between low-angle experimental and calculated structure factors for various model units (Fig. 2).

Thermal smearing corrections (Tanaka model) included.

Model	χ^2	R_w
Promolecule	24.2	0.0390
Sum of isolated molecules	16.4	0.0322
Model (*a*)	16.4	0.0321
Model (*b*)	15.4	0.0311
Model (*c*)	15.7	0.0315
Model (*d*)	15.2	0.0310

example, Jayatilaka & Chandler, 1997, and references therein).

2.5. Agreement parameters between experiment and theory

The primary quantity used to indicate the agreement between calculated structure factors, $F^c(\mathbf{k})$, and the experimental structure factors, $\mathbf{F}(\mathbf{k})$, is the χ^2 statistic,

$$\chi^2 = \frac{1}{N_r - N_p} \sum_{\mathbf{k}} \frac{[F^c(\mathbf{k}) - F(\mathbf{k})]^2}{\sigma(\mathbf{k})^2}. \quad (1)$$

N_r is the total number of unique reflections and N_p is the number of adjustable parameters used in the comparison (here, only one parameter, λ, is used, as described in paper I). $\sigma(\mathbf{k})$ are the assigned standard deviations in the experimental structure factors. It is very important to note that these are considered to be experimental measurements of equal importance to the structure factors themselves. It should also be noted that the signs of the experimental structure factors are not measurable. In our work, we have assigned the same sign to the experimental structure factors as the calculated structure factors. The weighted R factor

$$R_w = \frac{\sum_{\mathbf{k}} |F^c(\mathbf{k}) - F(\mathbf{k})|/\sigma(\mathbf{k})^2}{\sum_{\mathbf{k}} |F(\mathbf{k})|/\sigma(\mathbf{k})^2} \quad (2)$$

has also been included in Table 1 for comparison since it is often used as a measure of agreement in X-ray work, although only the χ^2 statistic was used in the fitting procedure. We prefer the χ^2 statistic since its relation to the accuracy of the X-ray data is clearer: a value $\chi^2 = 1$ indicates that, on average, the calculation is just within the acceptable experimental error bounds.

2.6. Electric potential

The electric potential is defined as

$$\varphi(\mathbf{r}) = \sum_k \frac{Z_k}{|\mathbf{r} - \mathbf{r}_k|} - \int \frac{\rho(\mathbf{r}')}{|\mathbf{r} - \mathbf{r}'|}\, \mathrm{d}\mathbf{r}', \quad (3)$$

where Z_k and $\mathbf{r}_k$ are the charge and position of nucleus k and $\rho(\mathbf{r})$ is the electron density at point $\mathbf{r}$.

2.7. Electron localization function

Electron-localization-function (ELF) (Becke & Edgecombe, 1990) plots may be characterized as functionals of a model wavefunction which produce regions in which 'pairs' of electrons may be discerned. The ELF is related to the smallness of the first term in a Taylor expansion of the spherically averaged conditional pair probability distribution for electrons of the same spin around a reference point; the smaller the probability of finding a second like-spin electron near the reference point, the more highly localized is the reference electron. Specifically,

$$\mathrm{ELF}(\mathbf{r}) = [1 + (D_\sigma/D_\sigma^0)^2]^{-1}, \quad (4)$$

where D_σ is the aforementioned first term in the spherically averaged conditional pair probability distribution,

$$D_\sigma = \tau_\sigma - \tfrac{1}{4}(\nabla\rho_\sigma)^2/\rho_\sigma, \quad (5)$$

and

$$\rho_\sigma = \sum_i^\sigma |\psi_i|^2 \quad (6)$$

$$\tau_\sigma = \sum_i^\sigma |\nabla\psi_i|^2. \quad (7)$$

The summation runs over the spatial parts of the orbitals of spin σ, which comprise a model single-determinant function. D_σ^0 is D_σ when evaluated for a uniform electron gas of density $\rho_\sigma(\mathbf{r})$, $D_\sigma^0 = \frac{3}{5}(6\pi^2)^{2/3}\rho_\sigma^{5/3}$. Since ELF plots require a model single-determinant function (*i.e.* orbitals), they represent information that cannot ordinarily be obtained from a standard analysis of X-ray charge densities.

The ELF can take values between zero and one, with zero corresponding to no electron pairing, meaning the reference electron is delocalized, and one meaning the electron is highly localized. The ELF plot is capable of explicitly showing regions that correspond to chemical structure corresponding to bonding electron pairs, lone pairs and shell structure (Savin *et al.*, 1991).

3. Unconstrained wavefunction calculations for the electron density in oxalic acid dihydrate

In this section, the results from theoretical calculations on the oxalic acid cluster, without any fitting procedure, are examined.

3.1. Comparison of electron densities calculated by the Hartree–Fock and the promolecule models with experiment

Fig. 1 is a plot of the calculated Hartree-Fock electron density for an oxalic acid molecule surrounded by the four nearest water molecules in the plane of the oxalic acid unit, from which spherically averaged atomic electron densities have been subtracted.

Examination of the difference density plot clearly shows a build-up of electron density relative to the spherical-atom model around the oxygen atoms, which can be associated with the location of the lone pairs of oxygen atoms. There is also an

increase in the density between the C—O and C—C bonds. The build up of charge on the hydrogen atoms is not centered on the nuclear position but instead shifted towards the nearest bonded oxygen atoms in both the oxalic acid and water molecules. This is in agreement with previous density-functional-theory (DFT) calculations on the same system (Krijn & Feil, 1988).

Table 1 shows the χ^2 and R_w agreement statistics between calculated and observed low-angle X-ray structure factors. As well as the fragment depicted in Fig. 1, other kinds of model fragment Hartree–Fock wavefunctions have been used, and are shown in Fig. 2. In the infinite crystal, the structure factors calculated from each of these fragments would be identical, owing to translational symmetry. However, they are different in the model because the model fragment calculations do not possess the full crystal symmetry. For comparison, we give agreement statistics for the promolecule calculation, similar to what might be calculated in a standard X-ray analysis. Since it is only a superposition of spherical atomic densities at the appropriate crystal lattice positions, the promolecule calculation does have full crystal symmetry. A calculation is also reported where the electron density of the crystal is given as a superposition of the densities calculated for the oxalic acid and water molecules separately. Finally, it should be mentioned that model (*a*) was used by Zobel *et al.* (1992) (although it would have made no difference in his promolecule density model) and model (*b*) was used by Krijn & Feil (1988) in their calculations. Model (*d*) is displayed in Fig. 1 and is the focus of our work.

As might have been expected, the worst agreement occurs for the promolecule model, which gave a χ^2 value of 24.2. That is, the calculated values are on average only within $24.2^{1/2} \approx 5$ times the acceptable error margin. An improvement occurs when the model is composed of the densities of separate oxalic acid and water units – although the χ^2 of 16.4 is still poor. Obviously, the effects of intramolecular electron-density rearrangements in the separate oxalic and water molecules are detectable by X-ray measurements. The χ^2 values for the different models (*a*)–(*d*), which all include some effects of *inter*molecular electron-density rearrangement, are quite similar, the χ^2 values all being in the range 15.2–16.4. We conclude that the effects of intermolecular electron-density rearrangement are significantly smaller than intramolecular density rearrangement but they are still experimentally discernible. Model (*a*) is barely different to the density that is the sum of molecular units, while model (*b*) is better than (*a*) by one χ^2 unit. From this, we can conclude that the water molecule in the positions depicted in model (*b*) have more effect on the oxalic acid unit than those in model (*a*). This might be justified because the O—H contact distance in position (*b*) is 2.5 Å, compared to 2.8 Å in the other positions. [Note that the water molecules in (*a*) and (*b*) are equivalent both in the crystal and in our fragment model because both these models possess inversion symmetry.] Model (*c*) is in some sense an average of models (*a*) and (*b*), and this is reflected in its χ^2 which lies between models (*a*) and (*b*), even though this fragment does not possess inversion symmetry. Model (*d*), which is surrounded by four water molecules, is slightly better than model (*b*) by 0.2 χ^2 units. Based on the χ^2 agreement statistic, the larger fragment (*d*) is a slightly more realistic model of the entire crystal than any of the other choices of fragment, a conclusion that might have been expected *a priori*. The relatively small difference between models (*c*) and (*b*) suggests that care must be taken in choosing the fragment wavefunction, since predicted errors due to loss of symmetry in the fragment are not necessarily reflected in the χ^2 value.

The R_w statistic reported in Table 1 mirrors the changes in the χ^2 statistics, but it is much less sensitive. We do not recommend its use for accurate electron-density work.

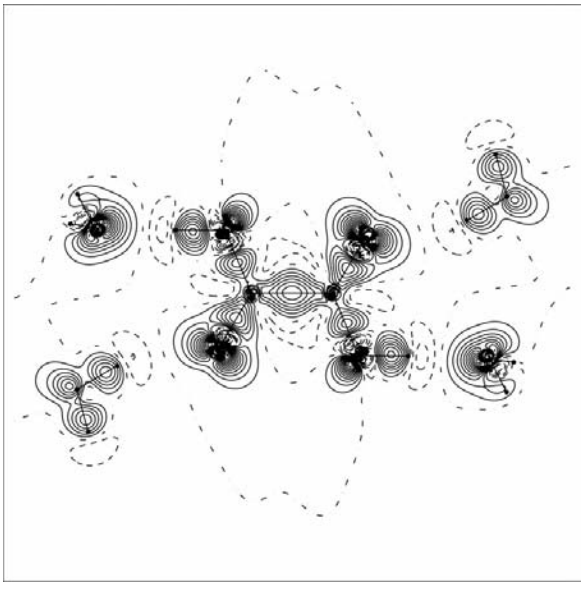

Figure 1
Hartree–Fock deformation electron density plot for an oxalic acid unit surrounded by four water molecules. Contours are at linear increments of 0.1 e Å^{-3}, with negative contours dashed, positive contours solid, zero contour dash-dotted.

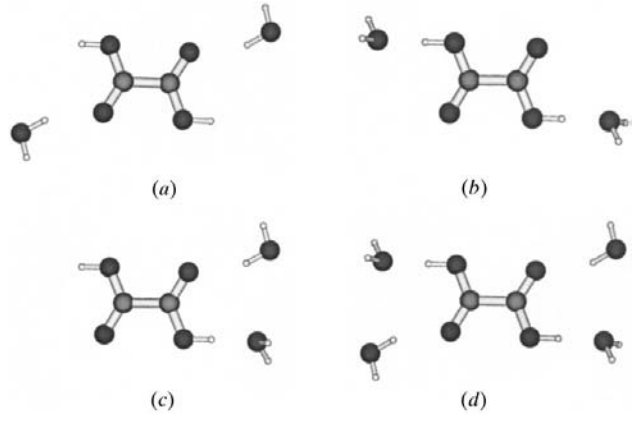

Figure 2
Different (but crystallographically equivalent) choices for the model units in the oxalic acid dihydrate crystal.

Table 2
χ^2 agreement statistic between low-angle experimental and calculated structure factors for various models (Fig. 2).

Calculated using different thermal smearing models.

	Thermal smearing model		
Model	Stewart	Coppens	Tanaka
Promolecule	24.2	24.2	24.2
Sum of isolated molecules	17.0	16.4	16.4
Model (*a*)	16.8	16.3	16.4
Model (*b*)	15.5	15.3	15.4
Model (*c*)	16.0	15.6	15.7
Model (*d*)	15.3	15.1	15.2

3.2. The effect of different thermal smearing models

In order to gauge the effect of thermal smearing corrections on the predicted structure factors, several thermal smearing models are compared in Table 2. The models given by Stewart (1969), Coppens *et al.* (1971) and Tanaka (1988) are compared in Table 2. Although all models produce χ^2 values within a range of 0.6 of each other, the Coppens model consistently gave the lowest χ^2, although only slightly better than the Tanaka model. The χ^2 for the promolecule density is not affected by the thermal smearing model, as shown in Table 2, as the three models are equivalent when there are no density-matrix elements between atoms.

The χ^2 agreement statistics without any correction for thermal smearing were of the order of 100 (even for the sum of atom densities). Therefore, thermal smearing corrections are essential and comparisons with experimental data that do not account for thermal motion are meaningless. Since the difference in χ^2 values between the different models is relatively small compared to the effect of no correction at all, it is less crucial which model is used for the correction. Thermal smearing corrections were subsequently applied in all further calculations, with the Tanaka model (Tanaka, 1988) being used since it is preferable for theoretical reasons (paper I).

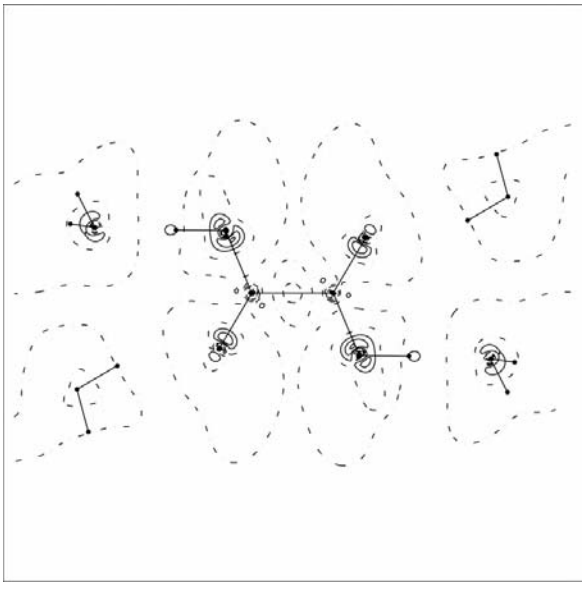

Figure 3
Difference between DFT and Hartree–Fock calculations for the electron density for an oxalic acid unit surrounded by four water molecules.

Table 3
χ^2 agreement statistic between low-angle experimental and calculated structure factors for various models (Fig. 2) calculated using Hartree–Fock and DFT methods.

Thermal smearing corrections (Tanaka model) included.

Model	HF	DFT
Sum of isolated molecules	16.4	12.8
Model (*a*)	16.4	12.7
Model (*b*)	15.4	11.5
Model (*c*)	15.7	11.9
Model (*d*)	15.2	11.5

3.3. The effect of different fragment partition models

Model (*d*) does not have the stoichiometry of oxalic acid dihydrate; there are four water molecules in this fragment. So that it conforms to the actual crystal, the density in the fragment must be divided between the oxalic acid and water molecules, weighting the density of each of the water molecules by a factor of one half in order to obtain the correct stoichiometry, and hence the correct X-ray structure factors. This, however, cannot be a unique procedure, as described in paper I. Two different partitioning models were used, the so-called equal-sharing basis-function method and the Gaussian-exponent unequal-sharing model, both discussed in paper I. To the accuracy of our χ^2, the results are identical for the two models, with a value of 15.2.

Another way to judge the quality of the partition model is to evaluate the theoretical value for the 000 reflection, which should be the total number of electrons in the unit cell, 132. The deviation for both models is very small, with both giving 132.07. These results suggest that the results obtained are stable relative to different partition models and in further calculations only the Gaussian-exponent unequal-sharing model was used.

3.4. Comparison of electron densities calculated by density-functional theory and the Hartree–Fock models

Having established that intramolecular charge-density redistribution may be detected by experiment, we now ask if electron correlation effects on the density can be discerned. To test this question, we have performed density-functional theory (DFT) calculations, which should include such effects. Certainly, DFT calculations for many related isolated molecular properties, including one-electron properties such as dipole moments and equilibrium geometries, are accurate (Johnson *et al.*, 1993).

The χ^2 agreement statistics for the various models are presented in Table 3. The χ^2 for the DFT calculated densities are consistently lower than for the corresponding Hartree–Fock results. Clearly, the effects of electron correlation can be discerned by the experiment. Again, however, the calculations are not within the acceptable experimental error range.

Fig. 3 shows the difference between the DFT and Hartree–Fock electron densities for the case of four water molecules, model (*d*). It shows a significant increase in the electron density near all oxygen atoms and a deficit nearer the nuclei of the oxygen and carbon atoms. The density between the two carbon atoms also appears to be overestimated by Hartree–Fock theory.

3.5. Effects on the electron density due to long-range crystal interactions

Since DFT is expected to give electron densities very close to the true electron density of a system, there are two possibilities as to why such a poor result was obtained. Either the DFT method is not accurate enough for this system or the oxalic acid unit surrounded by four water molecules is not sufficiently large to account for the electron density that might occur in an infinite crystal lattice.

To address this latter issue, the effects of the lattice environment were explored by including neighboring molecules in larger Hartree–Fock and DFT calculations. The cluster chosen comprised 7 oxalic acid and 10 water molecules, all within a distance of 8 atomic units of the midpoint of the C—C bond in the oxalic acid molecule. Fig. 4 is a pictorial representation of this cluster.

Fig. 5 is a DFT deformation density plot (relative to the promolecule reference) that shows the influence of neighboring molecules in the crystal. The deformation densities around each water molecule appear similar to the Hartree–Fock calculation comprised of one oxalic unit surrounded by four water molecules, model (*d*) in Fig. 1. There is a slight increase in density in the COH—O hydrogen bond, but this is also present in Fig. 3, indicating it is an intramolecular electron-correlation effect, rather than a crystal-lattice effect. The electron densities between the carbon and oxygen atoms and between the two carbon atoms of the central oxalic acid unit in the cluster are not as large as in the isolated Hartree–Fock electron density in Fig. 1, but again this is also a result of intramolecular electron correlation, as the difference is also present in Fig. 3. A plot of the difference between the Hartree–Fock and DFT densities for the cluster (not shown) was negligibly different to the same plot for the smaller cluster (Fig. 3). It appears that the effect of the neighboring molecules is not significant. This conclusion is supported by the values of the χ^2 agreement statistics between the experimental structure factors and the calculated structure factors obtained from the electron density of the central four-water unit of the cluster and in the isolated model (*d*) fragment. These are displayed in Table 4. When using the Hartree–Fock model, there is an improvement of 0.5 units in the χ^2 value owing to cluster effects, whereas, when using the DFT method, the improvement is 0.8 units. The effects of using density-functional theory instead of Hartree–Fock theory (*i.e.* intramolecular electron correlation), amounting to an improvement of about 3 units, is larger than these cluster effects.

Table 4
χ^2 agreement statistic between low-angle experimental and calculated structure factors for the DFT and Hartree–Fock densities for an oxalic acid crystal fragment in configuration (*d*) of Fig. 2 and for the extended cluster in Fig. 4.

Structure factors for the cluster were calculated from the electron density on the central symmetry-unique portion. Thermal smearing corrections (Tanaka model) included.

Model	χ^2
HF isolated	15.2
HF cluster	14.7
DFT isolated	11.5
DFT cluster	10.7

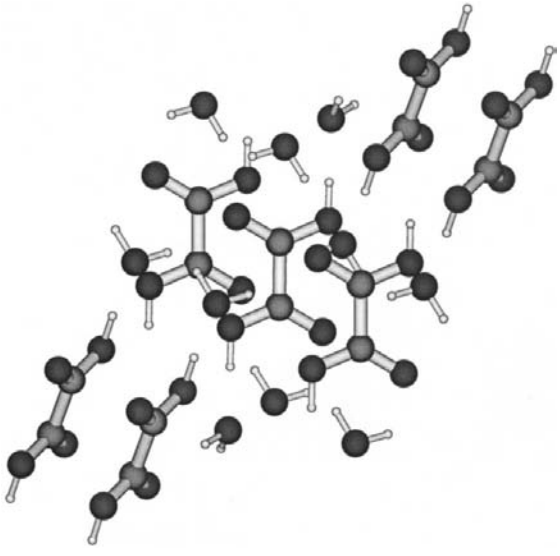

Figure 4
Geometrical configuration for the large oxalic acid dihydrate cluster calculation, involving all atoms within a radius of 8 atomic units of the midpoint of the C—C bond in the central oxalic acid unit.

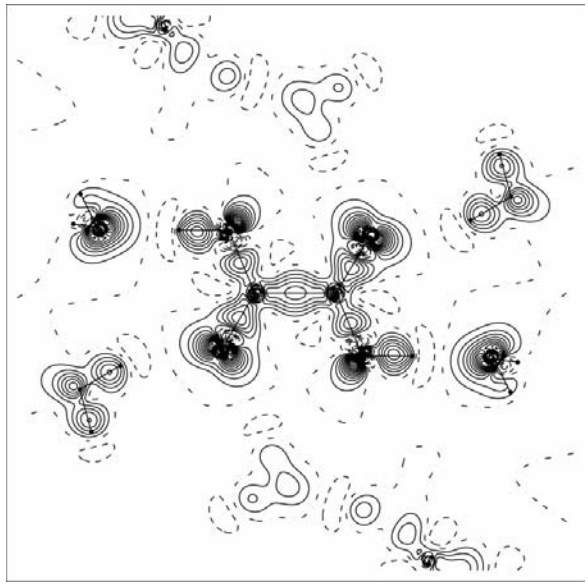

Figure 5
DFT deformation electron-density plot for an oxalic acid unit surrounded by six other oxalic acid units and ten water molecules within a radius of 8 atomic units.

Table 5
Variation of the χ^2 agreement statistic between low-angle experimental and calculated structure factors, the SCF energy E_{SCF} and the SCF kinetic energy T_{SCF} for an oxalic acid fragment in configuration (*d*) of Fig. 2 as a function of the Lagrange multiplier λ.

Energies in Hartrees. Thermal smearing corrections (Tanaka model) included.

λ	χ^2	E_{SCF}	T_{SCF}
0.00	15.2	−680.61	681.83
0.05	6.0	−680.50	681.90
0.10	4.8	−680.41	682.39
0.20	3.9	−680.28	683.27
0.30	3.4	−680.18	683.99

It appears that modeling long-range crystal interactions *via* DFT calculations still cannot account for the observed experimental data.

3.6. Effect of basis-set size on the agreement statistics with experiment

Basis-set size effects on the agreement statistics were determined by comparing Hartree–Fock model (*d*) calculations using DZP (Dunning, 1970) and cc-pVTZ (Dunning, 1989) basis sets. These calculations contained 210 and 500 basis functions, respectively.

The χ^2 using the DZP basis set was 15.2, while the χ^2 using the cc-pVTZ basis set was 14.3. To put this into perspective, the change is slightly more than the effect of long-range cluster effects and about the same to half the change observed due to short-range hydrogen-bonding effects obtained from different fragment partitions.

Plots in real space of the differences between the static densities from these two different basis sets (not presented) are very small, amounting to 0.2 e Å^{-3} in the carbonyl bond regions.

While it is encouraging that the results are improved for the calculation with a better basis set, the magnitude of the improvement is still far from that required to obtain experimental accuracy.

3.7. Comparison of the results with other work

The best calculations on this system to date have been provided by Krijn & Feil (1988), who performed (correlated) local density-functional calculations using very good triple-zeta Slater-type orbital basis sets. A comparison of their deformation-density plots (Fig. 2) with our gradient-corrected BLYP density-functional calculations (Fig. 1 plus Fig. 3) shows negligible differences.

Krijn & Feil (1988) have also made estimates of the effects of long-range crystal interactions on the density rearrangement in the oxalic acid molecule by embedding the oxalic acid molecule in an effective crystal potential. We have made plots (not presented) that show the effect of the long-range crystal effects on the density rearrangement from our cluster calculation. A comparison of these with those of Krijn & Feil (1988) (Fig. 4) show similar features but much less exaggerated. The changes are very small, with peaks at the 0.1 e Å^{-3} level.

4. An experimental wavefunction for the oxalic acid dihydrate crystal

In this section, the fragment wavefunction fitting method described in paper I is used to investigate some of the reasons why the previous calculations are not capable of reproducing the observed data.

4.1. Effects of the wavefunction fitting method on the agreement statistics

Fig. 6 is a plot of the effect of λ on the χ^2 agreement statistic when the wavefunction fitting procedure described in paper I is applied to the central oxalic acid unit surrounded by the four nearest water molecules (model *d*). There is a sharp decrease in the χ^2 initially with fitting, so even a small amount of fitting can significantly improve agreement with experiment. (The value $\lambda = 0$ corresponds to an unconstrained Hartree–Fock calculation.) Table 5 gives the corresponding numerical data. When $\lambda = 0.3$, the value of χ^2 is 3.4, reduced from an initial value of 15.2, and this is starting to approach experimental error bounds ($\chi^2 = 1$). The weighted *R* factor is reduced fom 0.0310 to 0.0147 with fitting. Fitting beyond the value $\lambda = 0.3$ proves difficult owing to numerical issues, as discussed in paper I. In order to effect reasonable convergence in the fitting calculations, the direct inversion of the iterative subspace (DIIS) scheme (Pulay, 1982) was used, along with the rescaling techniques described in paper I. Furthermore, instead of using the density matrix resulting from an iteration of the self-consistent field procedure, as is usually the case, the actual density used in each cycle comprised a combination of 70% of the old density matrix plus 30% of the new density matrix. That is, the density matrix was 'damped' by a factor of 0.7. This is important information for the reproduction of our work because the solution of the fitting equations is otherwise ill conditioned with increasing Lagrange multiplier, λ.

4.2. Effects on the agreement statistics for the complete structure-factor data set

The constraint used in our wavefunction calculations included only low-angle ($\sin\theta/\lambda < 0.71$ Å^{-1}) X-ray reflections as these contain most information about 'valence-electron' regions. To determine whether this assumption was valid, the

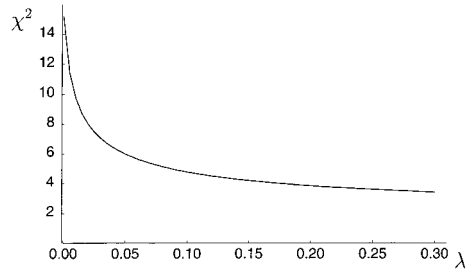

Figure 6
Variation of the χ^2 agreement statistic between low-angle experimental and calculated structure factors with the Lagrange multiplier λ for an oxalic acid crystal fragment in configuration (*d*) of Fig. 2. Thermal smearing corrections (Tanaka model) are included.

agreement statistic between the calculated and experimental structure factors was compared for the high-angle and full data sets. The results are shown in Table 6, with the promolecule model included for comparison.

The constraint to match the experimental low-angle data has also improved agreement with the high-angle data (and thus the full data set).

An interesting feature of Table 6 is that the promolecule gives the best agreement with the high-angle data. The original atomic parameters were refined (Zobel *et al.*, 1992) using atomic form factors on the high-angle data only, creating a bias toward atomic densities. This bias is not seen in the χ^2 for the low-angle data.

4.3. The energy, kinetic energy and orbital energies of the fitted wavefunction as a function of the Lagrange multiplier

Fig. 7 shows the behavior of the total and kinetic self-consistent field (SCF) energies as a function of the Lagrange multiplier λ. Table 5 contains numerical values for the figures. As expected, the Hartree–Fock energy in Fig. 7 increases as the constrained wavefunction moves away from the Hartree–Fock wavefunction. At $\lambda = 0.3$, convergence slowdown problems in the constrained fitting procedure became serious and so fitted wavefunctions for larger values of λ were not attempted. The energy change at $\lambda = 0.3$ is 1.13×10^6 J mol^{-1}, which is much more than the energy of a hydrogen bond, typically around 20×10^3 J mol^{-1}. However, the Hartree–Fock energy for the corresponding BLYP density-functional-theory wavefunction is -680.51 Hartrees, representing a difference of 10×10^3 J mol^{-1} from the Hartree–Fock result. The energy change associated with the fitting procedure is more than a factor of four larger than this value – which is a value that might be expected from the 'real' electron density. Any larger change would seem unreasonable.

Since the Lagrange multiplier λ is a measure of the sensitivity of the Hartree–Fock energy being minimized to changes in the constraint function, we can conclude that, for large λ, large changes in the Hartree–Fock energy (Fig. 7) are required to effect only small changes in the agreement statistic χ^2 (Fig. 6). This could be because the model is inadequate – for example, there are not enough basis functions or the Hartree–Fock model itself is inadequate. It could also be because the data – the experimental structure factors, the associated

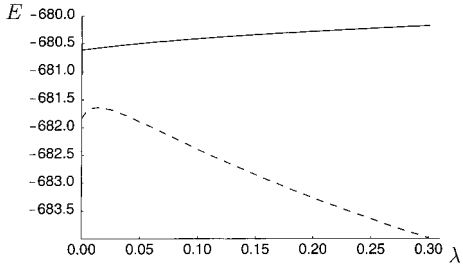

Figure 7
Variation of the fitted SCF energy (solid) and SCF kinetic energy (dashed) for an oxalic acid fragment in configuration (*d*) of Fig. 2 as a function of the Lagrange multiplier λ. (Energies in Hartrees.)

Table 6
The χ^2 agreement statistic between calculation and experiment for various structure-factor data sets.

The constrained Hartree-Fock wavefunction was fitted using the low-angle data set only. All data sets have reflections with $F < 2\sigma$ removed. Thermal smearing corrections (Tanaka model) included.

	Low angle $\sin\theta/\lambda < 0.71$ Å^{-1}	Full data set	High angle $\sin\theta/\lambda > 0.71$ Å^{-1}
Constrained HF	3.4	2.6	1.3
Unconstrained HF	15.2	9.8	1.6
Promolecule	24.2	15.0	1.1

experimental standard deviations or the refined parameters – are incorrect. In view of the already large energy change of the fitted wavefunction and the fact that even larger increases are to be anticipated for only small decreases in the χ^2 agreement statistic, it seems unrealistic to pursue a solution at higher λ even if this were possible.

Interestingly, the negative of the kinetic energy (Fig. 7) peaks near $\lambda = 0.015$ and then begins to decrease almost linearly to below the corresponding Hartree–Fock and BLYP values. The BLYP kinetic energy is 682.79 Hartrees, which is 0.96 Hartrees (2.5×10^6 J mol^{-1}) higher than the unconstrained Hartree–Fock result. The constrained Hartree–Fock kinetic energy is 2.16 Hartrees (5.7×10^6 J mol^{-1}) above the unconstrained result. The increasing kinetic energy indicates that, after $\lambda = 0.015$, the fitted electron density on average is becoming more 'bumpy' since the expectation value of ∇^2 is becoming larger. An examination of plots of the fitted electron density (discussed later) shows that these bumps may be associated with the increase in density at the closer hydrogen bond and an increase in density near the oxygen atom along the C—O bond.

Obviously, the kinetic energy is a sensitive function of fitting parameter λ. In a previous paper (Jayatilaka, 1998), it was suggested that the kinetic energy could be used, *via* the virial theorem, to obtain binding energies for the crystal. The sensitivity of the kinetic energy observed here would indicate that such an approach would not lead to reliable binding energies.

Canonical molecular-orbital energies were obtained for the fitted fragment wavefunction by diagonalizing the occupied–occupied block of the Fock matrix **f**, which was evaluated using the same molecular orbitals (the canonical molecular orbitals obtained this way are simply an orthogonal transformation of the fitted molecular orbitals). These fitted orbital energies were compared to the unfitted molecular-orbital energies for the same fragment. The mean deviation was 0.03 Hartrees and the maximum deviation was 0.10 Hartrees, with no obvious pattern to the deviations. The mean deviation of 66×10^3 J mol^{-1} is comparable to a strong hydrogen bond.

4.4. Effect of basis-set size on the constrained wavefunction fitting procedure

Owing to computational limitations, it was not possible to obtain a fitted wavefunction for the cc-pVTZ basis set.

Table 7
Variation of the χ^2 agreement statistic between low-angle calculated structure factors, the SCF energy E_{SCF} and the SCF kinetic energy T_{SCF} for an oxalic acid fragment in configuration (*d*) of Fig. 2 as a function of the Lagrange multiplier λ when fitting the DZP basis set to the cc-pVTZ BLYP structure factors.

Energies in Hartrees. Thermal smearing corrections (Tanaka model) included.

λ	χ^2	E_{SCF}	T_{SCF}
0.00	3.71	−680.61	681.83
0.10	0.52	−680.55	682.70
0.20	0.30	−680.52	683.31
0.30	0.21	−680.50	683.72
0.40	0.16	−680.48	684.02

Nevertheless, it is still very important to establish whether the DZP basis set we have used is sufficiently large and flexible to account for reasonable changes in the density, such as those that might be expected in the real system. (Recall that, in the case of *unfitted* wavefunction calculations, we already demonstrated that, although a larger basis set does yield better χ^2 agreement statistics, the improvement by itself is not sufficient to account for the disagreement with experiment.)

To address this question, we have attempted to fit the DZP wavefunction to the structure factors obtained from a correlated DFT calculation using model (*d*) with the cc-pVTZ basis. Table 7 shows the results. It is observed that χ^2 values of 0.16 are readily obtained by the fitting procedure, with only a small change in the reference Hartree–Fock energy. Difference density plots (not presented) between the two sets of calculated thermally averaged structure factors are extremely flat, with a maximum deviation of 0.03 e Å^{-3}. Obviously, the DZP basis set is sufficiently flexible to account for structure factors obtained from higher-level calculations.

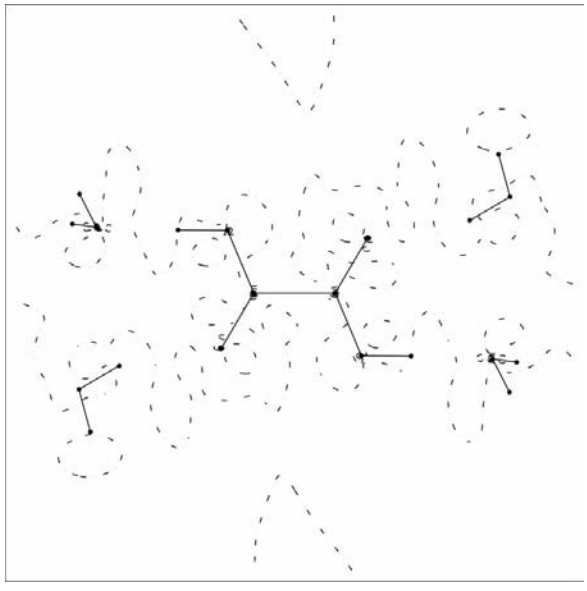

Figure 8
Difference in electron density between a wavefunction fitted to the experimental data and a wavefunction fitted with synthetically generated errors (see §4.5). The Lagrange multiplier λ was 0.3.

Note that the energy change obtained due to this fitting procedure was about 334×10^3 J mol^{-1}, again much smaller than the change of 1.1×10^6 J mol^{-1} observed for the wavefunction that was fitted to the experimental data.

4.5. Sensitivity of the fit to errors in the data

In order to test whether our procedure is stable to errors in the data, synthetic data were generated by adding artificial errors to each experimental structure factor obtained by Zobel. These errors were taken from a normal distribution with variance given by the experimental standard deviation (Press *et al.*, 1992). The overall χ^2 statistic between the experimental and synthesized data sets was 1.14. We were able to fit to the synthetic experimental data, and Fig. 8 shows the difference between our synthesized fit and the fit using the real experimental data. Both fits were performed at $\lambda = 0.3$, with a χ^2 of 4.3 for the synthesized data and 3.4 for the experimental data. There is little noise in Fig. 8, with near-zero deviation, except for around the carbon and oxygen nuclei, with the largest deviations in these atomic core regions being 0.6 e Å^{-3}. The pictures obtained from the fitting method are therefore not sensitive to random errors in the data.

4.6. An estimation of the remaining errors in the constrained-fitted wavefunction model

The best value of the χ^2 we have obtained after fitting was 3.4, which is still significantly short of the experimental error. It is of interest to discover if there is any systematic cause for this remaining discrepancy.

Fig. 9 is a scatter plot of the difference between the experimental and fitted wavefunction structure factors normalized by the experimental standard deviation against the scattering angle. Most of the deviations are clustered in the -5σ to $+5\sigma$ range without any obvious angle dependence. However, there are 11 calculated structure factors that lie over 5σ from the experimental value, the majority of which have low reflection angles. A plot of the same normalized deviations between the experimental and model structure factors against the experimental structure-factor magnitudes, shown

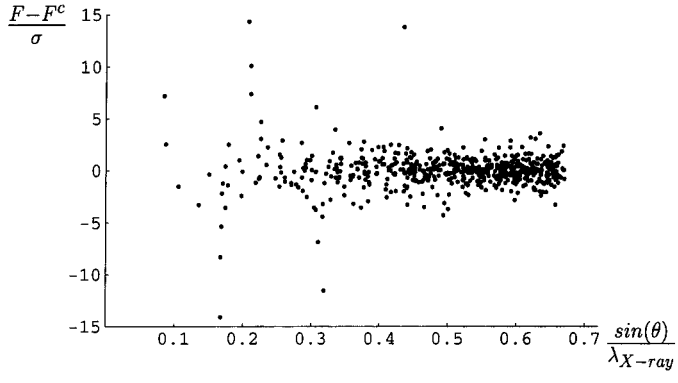

Figure 9
Variation of the experimental and calculated structure factors weighted by the experimental errors *versus* the scattering angle for the constrained ($\lambda = 0.3$) Hartree–Fock wavefunction. Only fitted structure factors ($\sin\theta/\lambda < 0.71$ Å^{-1}) are shown.

in Fig. 10, indicates that more than half of these poorly modeled reflections are very strong. If these 11 data are removed from the experimental data set, χ^2 is reduced from 3.4 to 1.5, or within a factor of $1.5^{1/2} = 1.2$ standard deviations of experiment. It appears that a few reflections have an inordinate effect on the χ^2 statistic.

Although a secondary-extinction correction was applied to the experimental data, such a correction necessarily depends on the choice of model structure factors (see paper I). The possibility that this extinction correction could be improved by using our fitted model wavefunction structure factors was investigated by applying again the correction of Larson (1970). It is easily shown that two applications of the Larson correction are the same to first order as a single correction with a corrected extinction factor, provided that the effect is small. The mean change in the calculated structure factors was 0.25%, which is indeed small. However, the χ^2 agreement statistic was significantly improved to 2.8. Obviously, there is strong incentive to use data where secondary-extinction effects are minimized, if possible.

It might be hoped that the agreement with experiment would be improved by removing the 11 outlying experimental data points and then by using an extinction correction on the remaining data. In fact, χ^2 remains at 1.5, *i.e.* the extinction correction appears to be completely dominated by these few reflections. This is consistent with the fact that these reflections tend to be strong and it is the strong reflections that are most affected by the extinction model.

The effect of basis-set incompleteness can also be estimated: the results in §4.4 demonstrated that the effect of using a larger basis set could amount to $0.16^{1/2} \approx 0.4$ experimental standard deviations. A constrained wavefunction fit using an experimental data set pruned of the 11 outlying data points, and also with a larger cc-pVTZ basis, might be expected to reach a goodness of fit of $0.8 = 1.2 - 0.4$, *i.e.* within experimental error. It must also be remembered that further improvement in the χ^2 could be obtained by using thermal smearing tensors and geometric positions that were optimized within the constrained wavefunction approach.

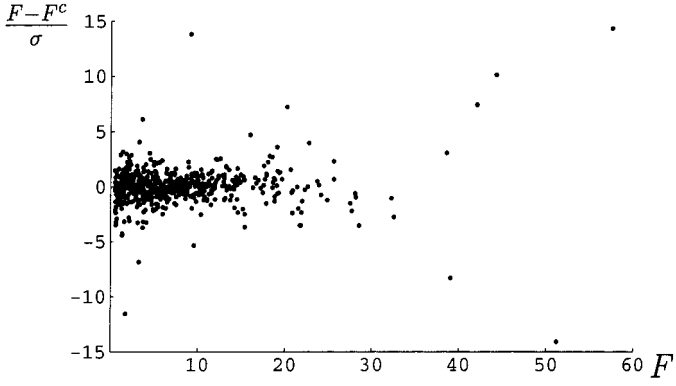

Figure 10
Variation of the experimental and calculated structure factors weighted by the experimental errors *versus* the experimental structure factors for the constrained ($\lambda = 0.3$) Hartree–Fock wavefunction. Only fitted structure factors ($\sin\theta/\lambda < 0.71$ Å^{-1}) are shown.

4.7. Effects on the electron density due to wavefunction fitting

Fig. 11 is the deformation density calculated by subtracting from the constrained Hartree–Fock wavefunction at $\lambda = 0.3$ for the fragment in model (*d*) (see Fig. 2) a sum of spherical atom densities for the same unit. Comparing this with Fig. 1 reveals a number of differences that are present in the experimental data but not correctly modeled by the Hartree–Fock calculation. These differences are probably more easily discerned in Fig. 12, which is a plot of the difference between the densities of the constrained and unconstrained Hartree–Fock calculations.

The most significant change occurs on the OH segment of the oxalic acid molecule, where there is a significant shift in density onto the hydrogen atom of the oxalic acid unit, presumably due to the nearby oxygen on the water molecule. In fact, there is a strong decrease in the electron density of this perturbing oxygen atom on the side nearest to this hydrogen atom of the oxalic acid unit. There is a depletion of charge in the lone-pair regions of the terminal oxygen molecule in the oxalic acid unit, and a simultaneous increase in the density close to the same oxygen atom, but along the CO bond. An almost identical but somewhat less pronounced depletion occurs on the non-terminal oxygen atom of the oxalic acid unit. A depletion of electron density is observed in one of the OH bonds of the water molecule, which is nearly in the plane of the plot. Finally, the density between the two carbon atoms in the oxalic acid molecule is decreased in the fitted wavefunction.

Since many of the density redistributions appear to involve the oxalic acid moiety only – that is, are intramolecular in nature – it might be expected that these effects could be accounted for by a better DFT calculation. Comparing Fig. 3, which shows only the effect of the DFT calculation relative to

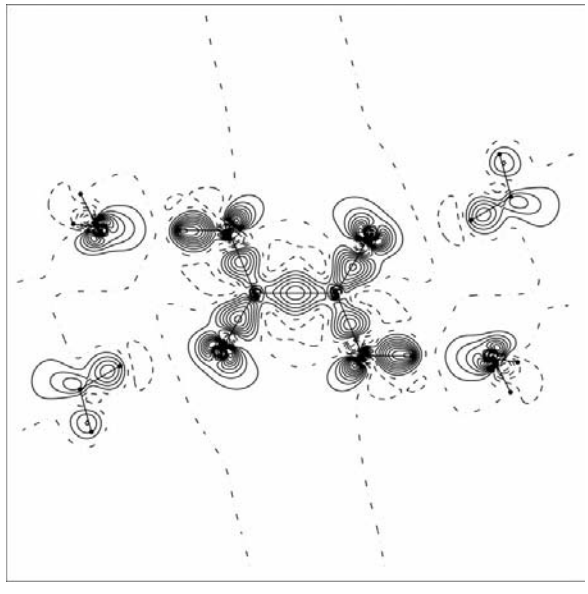

Figure 11
Constrained ($\lambda = 0.3$) Hartree–Fock deformation density plot for an oxalic acid unit surrounded by four water molecules.

the Hartree–Fock calculation, with the effect of the experimental data on the Hartree–Fock wavefunction, we do see some similarities in the density rearrangements on the oxygen atoms of the oxalic acid unit. However, density from the fitted wavefunction shows a much more pronounced effect. Similarly, the density increase on the hydrogen atoms of the oxalic acid unit show an increase in density in both plots, but it is significantly more pronounced in the fitted wavefunction calculation. Interestingly, the water molecule in the plane of the plot is similar for the Hartree–Fock and DFT densities, while, as mentioned already, the fitted wavefunction shows a moderate displacement of density.

In summary, it appears that some of the intramolecular density rearrangements can be explained qualitatively but not quantitatively by accurate calculations on the small cluster. Effects due to the interaction of the separate oxalic and water moieties involving redistribution of charge around the hydrogen atoms cannot be explained.

4.8. Structure-factor error maps

Instead of studying the electron density evaluated from the fitted wavefunction, we can look at the electron density as a result of the reverse Fourier transform of the structure factors. In this way, difference plots can be constructed directly from the measured and calculated structure factors, giving the error maps. (Recall that thermal smearing effects are included in the theoretical calculations.)

Figs. 13 and 14 are the error maps for the unconstrained and constrained wavefunction calculations, including all observed X-ray reflections. High-angle X-ray data have been included in order to accurately reproduce the core-electron regions, even though these data were not used in the fitting procedure. A comparison of these two maps shows that the fitting procedure has discernibly improved the agreement with the experimental electron density. The difference between these two maps is consistent, although not as pronounced, with the difference in the densities calculated directly from the wavefunctions (Fig. 12); in particular, there is an increase in density in the carbonyl bonds and an increase in density on the hydrogen atoms of the oxalic acid molecule. The lack of pronounced features occurs because these maps include the effect of thermal smearing, whereas the plots from the wavefunction do not. The lack of contours near the carbon and oxygen nuclei in Figs. 13 and 14 indicates that the DZP Gaussian basis set is able to reliably model these regions of the plot. The difference in density from experiment near the oxalic acid hydrogen atoms is reduced significantly in the fitted wavefunction, although still present.

4.9. Comparison of the results with other work

Using 100 K X-ray data, Krijn *et al.* (1988) have performed similar calculations to our own, examining the influence of intermolecular interactions on the electron density using the multipole fitting model. Essentially the same technique was used: experiment was compared to different theoretical models, which successively accounted for intramolecular effects, hydrogen-bonding effects and then finally long-range crystal effects, using agreement statistics and plots in real space. One complication in their study was that the multipole model cannot be transformed continuously into the theoretical model *via* a parameter λ, as in our approach. In order to effect an unbiased comparison with experiment, these authors were forced to use the multipole model to fit to the theoretical data and experimental data in a complicated iterative process

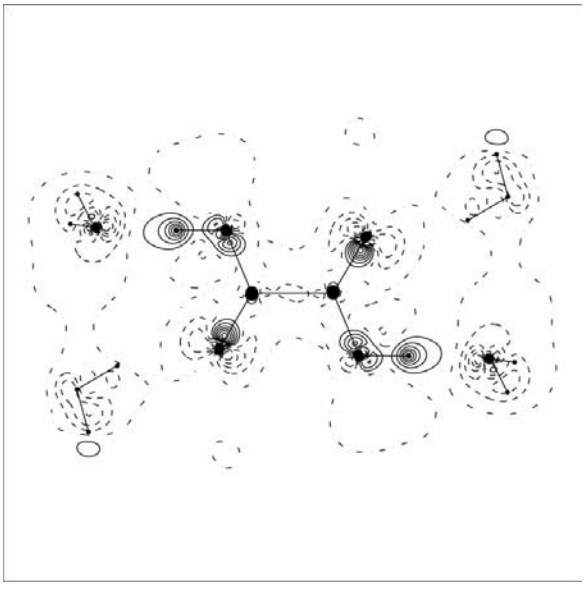

Figure 12
Difference between the constrained ($\lambda = 0.3$) and unconstrained Hartree–Fock static density plots for an oxalic acid unit surrounded by four water molecules.

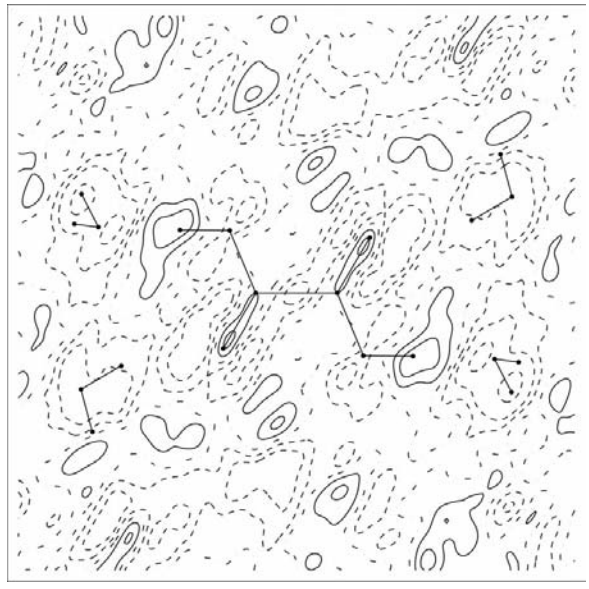

Figure 13
Error map generated by the inverse Fourier transform of the difference between the experimental and unconstrained Hartree–Fock structure factors. All experimentally observed structure factors are used. Contours are at linear increments of 0.05 e Å^{-3} with negative contours dashed, positive contours solid, zero contour dash-dotted.

designed primarily to obtain a consistent set of thermal parameters and a correct absolute scale factor for the experimental X-ray data. Nevertheless, after this procedure they came to the same conclusion as us, that hydrogen bonding and long-range crystal interaction are discernible in the fit statistics obtained from X-ray data. Plots of the difference between the final fit between the experimental and theoretical thermally averaged electron density showed deviations peaking at 0.15 e $Å^{-3}$ [(Krijn *et al.*, 1988), Fig. 6]. The deviations we observe with our fitting model (Fig. 14) using the data of Zobel peak similarly at 0.12 e $Å^{-3}$. Our fitting model, which involves only one adjustable parameter, is therefore comparable in agreement to the model of Krijn *et al.* (1988) but fitted to the better 15 K temperature data of Zobel.

4.10. Electron localization plots

Fig. 15 is the electron-localization-function (ELF) plot for the fitted model (*d*) wavefunction in Fig. 2. It shows significant electron localization in the hydrogen bond between the two water molecules closest to the oxalic acid unit, but virtually no hydrogen bond for the other two water molecules with the oxalic acid unit. The localization of the hydrogen bonds is small compared to the localization due to intramolecular bonding. The lone pairs on all oxygen atoms are seen. The shell structure of the oxygen and carbon atoms are indicated by the circular regions separated by many contours close to the nuclei.

An interesting feature of Fig. 15 is the localization away from the water molecule in the top-right corner of the plot. There is another oxalic acid molecule at this position in the crystal, suggesting a deficiency in the model (*d*) fragment wavefunction in representing the extended crystal density.

4.11. Electric potential plots

Fig. 16 is a plot of the difference in electric potential between the constrained and unconstrained Hartree–Fock wavefunctions. The maximum difference of 0.13 atomic units occurs on the water molecules. The differences are similar to the difference in electron density between the same wavefunctions (Fig. 12) except around the carbon atoms. The carbon atoms do not show any significant difference in Fig. 12, whereas the electric potential around them in the constrained Hartree–Fock wavefunction is significantly less. It should be noted that Fig. 16 shows the difference in potential for a fragment unit of the crystal, which is not the same as the potential of the unit in the complete crystal environment. Nevertheless, there are significant differences in the electric potentials obtained from the fitted and isolated fragments. This has important implications for the rational design of molecular crystal structures from isolated molecular units using the electric potential as a basis.

5. Conclusions

We have shown that it is possible to obtain model experimental wavefunctions for the oxalic acid dihydrate molecule, as it occurs in the crystalline form, by fitting to accurate X-ray data. The computational requirements are not extreme and are of the same order as a regular SCF calculation of the same unit, although convergence problems arise when the fitting parameter λ is large.

The best fit we obtain for the low-angle reflection data yielded a χ^2 value between the calculated and observed structure factors of 3.4. However, most of this error is due to only a few reflections in the experimental data set. If these are

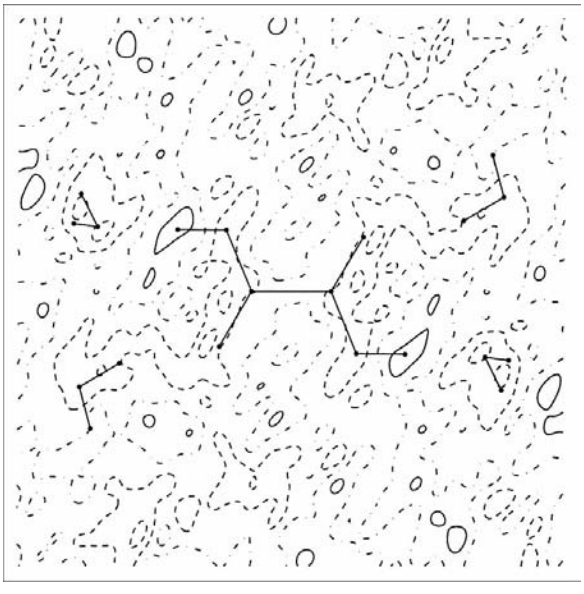

Figure 14
Error map generated by the inverse Fourier transform of the difference between the experimental and constrained ($\lambda = 0.3$) Hartree–Fock structure factors. All experimentally observed structure factors are used.

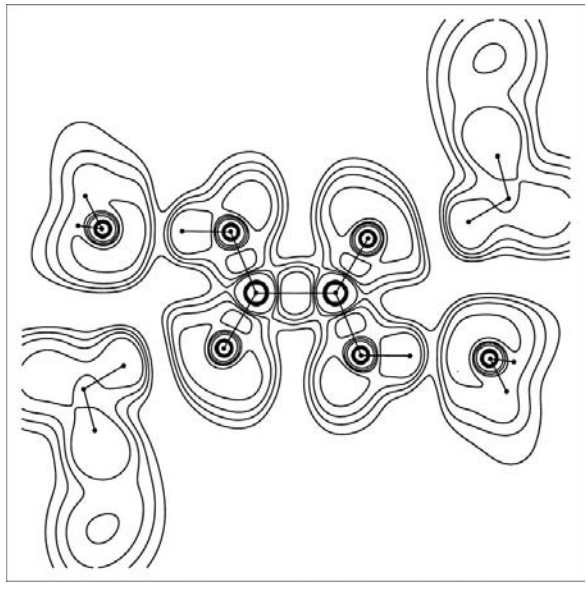

Figure 15
Electron-localization-function (ELF) plot for the constrained ($\lambda = 0.3$) Hartree–Fock wavefunction for the oxalic acid unit surrounded by four water molecules. Contours are at linear increments of 0.2 atomic units with the outermost contour being 0.2 atomic units.

removed, χ^2 is reduced to 1.5. The remaining error could be due to basis-set incompleteness but other effects such as small changes in the geometric positions of certain atoms in the crystal or the use of non-optimum thermal smearing parameters in the model could also be the cause. Based on these considerations, it seems likely that the reason we are not able to obtain a better χ^2 value than 3.4 without convergence problems is that any remaining improvement in the agreement would be either unphysical (owing to the attempted fitting of outlying data) or unobtainable within the basis set used for fitting. It should be remembered in this regard that the basis set used for fitting here is much more flexible than that normally used in so-called multipole models for the charge density.

It is clear, however, that the remaining errors in the χ^2 statistic have little effect on the dynamic electron-density maps constructed from the experimental data by our fitting technique (at least to an error of 0.1 e Å^{-3}).

It is more problematic to explain the disagreement with experiment and the unfitted *ab initio* wavefunction calculations. After an exhaustive analysis of the resulting unfitted electron-density plots, significant discrepancies remain between the experimentally observed densities (after fitting) and those from *ab initio* calculations of the gas-phase molecule. In particular, the effects of hydrogen bonding, which can clearly be seen in the constrained wavefunction calculations, are not properly accounted for by the Hartree–Fock model, nor by a supposedly more accurate model obtained from density-functional theory. The possibility that these discrepancies could be due to long-range crystal effects is also unlikely based on our calculation of an extended cluster of oxalic acid and water molecules.

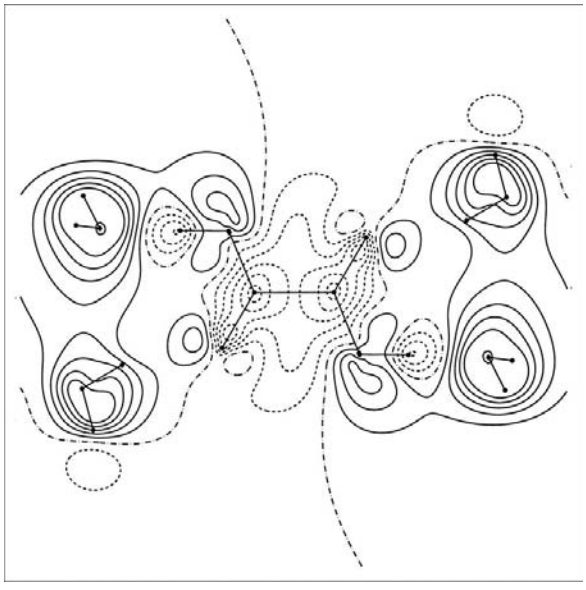

Figure 16
Difference between the electric potential of the constrained ($\lambda = 0.3$) and unconstrained Hartree–Fock wavefunctions for the oxalic acid unit surrounded by four water molecules. Contours are at linear increments of 0.02 atomic units, with negative contours dashed, positive contours solid, zero contour dash-dotted.

It is possible that some intermolecular density redistribution might be explained by small changes in geometric parameters, as for the fitted wavefunctions. Some electron-density redistribution may also be due to intermolecular electron correlation effects that were not accounted for correctly by the density-functional-theory calculations. Fully periodic crystal calculations are needed (rather than cluster calculations) to examine properly the effects of long-range crystal interactions on the electron redistributions in the isolated fragment, but such calculations are problematic for large basis sets. Another problem is that fully periodic calculations such as available in *CRYSTAL98* (Dovesi *et al.*, 1998) do not routinely include the empirical thermal smearing corrections that are essential for accurate comparison. Further work is also required in order to eliminate all these possibilities.

One important aspect of this work is that, once an experimental wavefunction is available, many interesting experimentally derived properties can be obtained simply as expectation values of operators, in the usual way required by quantum mechanics. Here we have only explored the kinetic and total energies, pseudo-orbital energies, the electric potential and the electron localization function. The possibility to exploit these experimentally derived properties for materials science studies is obviously an important long-term application of the experimental wavefunction analysis technique.

DJ acknowledges funding from the Australian Research Council QE-II fellowship scheme. DJG acknowledges funding from an Australian Postgraduate Award.

References

Becke, A. D. (1988). *Phys. Rev. A*, **38**, 3098–3100.
Becke, A. D. & Edgecombe, K. (1990). *J. Chem. Phys.* **92**, 5397–5403.
Coppens, P., Willoughby, T. V. & Csonka, L. N. (1971). *Acta Cryst.* A**27**, 248.
Dovesi, R., Saunders, V. R., Roetti, C., Causà, M., Harrison, N. M., Orlando, R. & Zicovich-Wilson, C. M. (1998). *CRYSTAL 98 Users Manual.* University of Torino, Torino, Italy.
Dunning, T. H. (1970). *J. Chem. Phys.* **53**, 2823–2833.
Dunning, T. H. (1989). *J. Chem. Phys.* **90**, 1007–1023.
Frisch, M. J., Trucks, G. W., Schlegel, H. B., Scuseria, G. E., Robb, M. A., Cheeseman, J. R., Zakrzewski, V. G., Montgomery, J. A., Stratmann, R. E. Jr, Burant, J. C., Dapprich, S., Millam, J. M., Daniels, A. D., Kudin, K. N., Strain, M. C., Farkas, O., Tomasi, J., Barone, V., Cossi, M., Cammi, R., Mennucci, B., Pomelli, C., Adamo, C., Clifford, S., Ochterski, J., Petersson, G. A., Ayala, P. Y., Cui, Q., Morokuma, K., Malick, D. K., Rabuck, A. D., Raghavachari, K., Foresman, J. B., Cioslowski, J., Ortiz, J. V., Baboul, A. G., Stefanov, B. B., Liu, G., Liashenko, A., Piskorz, P., Komaromi, I., Gomperts, R., Martin, R. L., Fox, D. J., Keith, T., Al-Laham, M. A., Peng, C. Y., Nanayakkara, A., Gonzalez, C., Challacombe, M., Gill, P. M. W., Johnson, B., Chen, W., Wong, M. W., Andres, J. L., Gonzalez, C., Head-Gordon, M., Replogle, E. S. & Pople, J. A. (1998). *Gaussian 98*, Revision A.7. Gaussian, Inc., Pittsburgh, PA, USA.
Jayatilaka, D. (1998). *Phys. Rev. Lett.* **80**, 798–801.

Jayatilaka, D. & Chandler, G. S. (1997). *Mol. Phys.* **92**, 471–476.
Jayatilaka, D. & Grimwood, D. J. (2001). *Acta Cryst.* A**57**, 76–86.
Johnson, B. G., Gill, P. M. W. & Pople, J. A. (1993). *J. Chem. Phys.* **98**, 5612–5626.
Krijn, M. P. C. M. & Feil, D. (1988). *J. Chem. Phys.* **89**, 4199–4208.
Krijn, M. P. C. M., Graafsma, H. & Feil, D. (1988). *Acta Cryst.* B**44**, 609–616.
Larson, A. C. (1970). In *Crystallographic Computing*, edited by F. R. Ahmed, pp. 291–294. Copenhagen: Munksgaard.
Lee, C., Yang, W. & Parr, R. G. (1988). *Phys. Rev. B*, **37**, 785–789.
Press, W. H., Teukolsky, S. A., Vetterling, W. T. & Flannery, B. P. (1992). *Numerical Recipes in Fortran 77*, 2nd ed., pp. 279–280. Cambridge University Press.
Pulay, P. (1982). *J. Comput. Chem.* **3**, 556.
Savin, A., Becke, A. D., Flad, J., Nesper, R., Preuss, H. & von Schnering, H. G. (1991). *Angew. Chem. Int. Ed. Engl.* **30**, 409–412.
Stewart, R. F. (1969). *J. Chem. Phys.* **51**, 4569–4577.
Tanaka, K. (1988). *Acta Cryst.* A**44**, 1002–1008.
Zobel, D. (1996). Private communucation.
Zobel, D., Luger, P., Dreissig, W. & Koritsanszky, T. (1992). *Acta Cryst.* B**48**, 837–848.